Received: 17 February 2017 | Revised: 25 May 2017 | Accepted: 2 July 2017

DOI: 10.1002/stc.2072

RESEARCH ARTICLE

WILEY

Energy regenerative tuned mass dampers in high-rise buildings

Wenai Shen[1,2] | Songye Zhu[2] | You-Lin Xu[2] | Hong-ping Zhu[1]

[1]School of Civil Engineering and Mechanics, Huazhong University of Science and Technology, Wuhan, China

[2]Department of Civil and Environmental Engineering, The Hong Kong Polytechnic University, Kowloon, Hong Kong

Correspondence
Songye Zhu, Department of Civil and Environmental Engineering, The Hong Kong Polytechnic University, Kowloon, Hong Kong.
Email: ceszhu@polyu.edu.hk

Funding information
National Natural Science Foundation of China, Grant/Award Number: 51508217 and 51629801; Hong Kong Polytechnic University, Grant/Award Number: 1-ZVJS; Research Grants Council of Hong Kong, Grant/Award Number: PolyU 5330/11E

Summary

This study investigates a novel energy regenerative tuned mass damper (TMD) with dual functions—vibration control and energy harvesting—in a high-rise building. The energy regenerative TMD consists of a pendulum-type TMD, an electromagnetic damper, and an energy-harvesting circuit. A simple optimal design method for energy regenerative TMD is proposed, in which a fixed duty-cycle buck-boost converter is employed as the energy-harvesting circuit to optimize the energy-harvesting efficiency and damping coefficient of the TMD. This study is organized into two main tasks: (a) characterizing and modeling the energy regenerative TMD through laboratory testing of a scaled prototype and (b) evaluating the vibration control and energy-harvesting performance of the energy regenerative TMD when applied in a 76-story wind-excited benchmark building in consideration of the nonlinearities in the energy regenerative TMD. The simulations reveal that the harvested electric power averages from hundreds of watts to kilowatts level when the mean wind speed ranges 8–25 m/s. Meanwhile, the building vibration is mitigated with the control performance comparable to the optimally designed passive TMD in a wide range of wind speed. The results in this study clearly demonstrate the effectiveness of the dual-function energy regenerative TMD when applied to building structures.

KEYWORDS

benchmark building, electromagnetic damper, energy harvesting, energy regenerative tuned mass damper, Simulink model, vibration control

1 | INTRODUCTION

Strong winds may cause excessive vibrations of high-rise structures and adversely affect occupant comfort and structural safety. Tuned mass damper (TMD) is one of the best-known solutions to suppress wind-induced vibrations of buildings and towers.[1–14] Soto and Adeli[12] conducted a comprehensive review on the applications of TMDs in high-rise buildings and towers. Very recently, a novel type of TMD, termed energy regenerative TMD, was proposed for both vibration control and energy-harvesting functions.[14–24] The energy-dissipating dampers in conventional TMDs are replaced by electromagnetic (EM) dampers,[25–28] which convert a portion of damping energy into electric energy to be harvested and stored by an energy-harvesting circuit (EHC).[27,28] Such energy-harvesting strategy avoids dissipating energy to heat and offers renewable energy to power vibration monitoring or control system.

The energy regenerative TMD is based on the concept of regenerative dampers that was first introduced in the field of mechanical engineering in the 1970s.[29–34] The emerging energy-harvesting function enables the traditional control or monitoring systems to evolve towards self-powered and autonomous systems. The idea of applying energy regenerative TMDs in civil structures was independently proposed by Zhu et al.,[14] Cassidy et al.,[15] and Ni et al.[16] in 2011. The full-scale performance of energy regenerative TMDs was numerically investigated using oversimplified models or circuits.[14,16] Cassidy et al.[15] demonstrated the energy-harvesting function of an energy regenerative TMD using a real-time hybrid testing method. The authors of this paper also experimentally verified that a small-scale energy regenerative TMD can harvest electricity to power a commercial wireless sensor.[17] In addition, some researches put forward self-powered adaptive or semiactive control system on the basis of energy regenerative TMD.[19,21] The optimal design of an energy regenerative TMD represents a dual-objective optimization problem that should address vibration control and energy-harvesting functions simultaneously. Harne[18] numerically searched the optimal mass ratio and load resistance of a linear EM oscillator installed on a panel and found that the optimal parameters for the two objective were not identical under harmonic excitations and the output power was comparatively insensitive to the mass ratio and load resistance. A similar result was reported by Gonzalez-Buelga et al.[19] who concluded that a smaller mass ratio of energy regenerative TMD provides higher power to harvest when considering harmonic base excitations. However, when considering white noise input, the optimal parameters for vibration control and energy harvesting are very close to each other.[20]

Although the general control principle of energy regenerative TMDs is similar to that of conventional TMDs, the new energy-harvesting function introduces more complex electronic dynamics into the whole system than does the conventional one. The characteristics of EHC affect not only its energy-harvesting performance but also its vibration control performance. Previous studies[14,16] tended to considerably overestimate the vibration control and energy-harvesting performance because various mechanical and electric loss and the nonlinearities in circuits and EM devices were overlooked. Consequently, the optimal design strategy for energy regenerative TMDs in consideration of the actual dynamics and nonlinearities in EM damper and EHC has yet to be established.

Therefore, this paper presents a comprehensive study on the modeling, optimal design, and full-scale performance evaluation of a pendulum-type energy regenerative TMD by fully considering the nonlinearities of EM damper and EHC. Section 2 presents the configuration of the proposed pendulum-type energy regenerative TMD. Section 3 establishes the dynamic model of the pendulum-type energy regenerative TMD in the Matlab Simulink environment on the basis of the laboratory testing to fully simulate its nonlinear behaviors. Section 4 presents a simple optimal design method of the energy regenerative TMD by considering the nonlinearities in the damper and circuit. Finally, the performance of a pendulum-type energy regenerative TMD applied to a 76-story wind-excited benchmark building is investigated with fully considering the nonlinearities of EM damper and EHC. The structural vibration control effect and energy-harvesting efficiency are discussed in detail.

2 | CONFIGURATION OF ENERGY REGENERATIVE TMD

A TMD is intrinsically a resonant oscillator whose frequency is tuned to be close to the target mode of the primary structure.[1–7] Hence, TMD shares common characteristics with a general single-degree-of-freedom (SDOF) energy harvester whose frequency is also tuned in accordance with ambient vibration sources.[35–40] This similarity inspires the concept that the conventional TMD can serve as a large-scale energy harvester if its damping energy could be converted into electrical energy. With the advancement from "energy dissipation" strategy to "energy-harvesting" strategy, conventional TMD evolves into an energy regenerative TMD that is essentially a dual-function system that performs both vibration mitigation and energy harvesting.[14–21]

Cable-supported or rigid-hanger-supported pendulums are a common form of conventional TMD.[4,7,8] In this study, the configuration with a mass hanged by a rigid bar to drive a damper installed at the pivot of pendulum is adopted, as shown in Figure 1(a). The pendulum-type energy regenerative TMD system consists of a rotary EM damper, a gear box, a pendulum, and an EHC, where the EM damper is a key component. Any permanent-magnet motors or generators can function as passive rotary EM dampers.[15,17,41] As shown in Figure 1(a), the rotational velocity of the pendulum is accelerated by a gear box, resulting in a large output damping torque T_d. As a result, the damping density of the pendulum-type TMD can be significantly enhanced.[17,41] The EM damper generates voltage waveforms through the pendulum motion, and the vibration energy is converted into electrical energy. A properly designed EHC connected to the EM damper output port is required to process the damper output energy before the electrical energy can be finally stored in a rechargeable battery or supercapacitor.

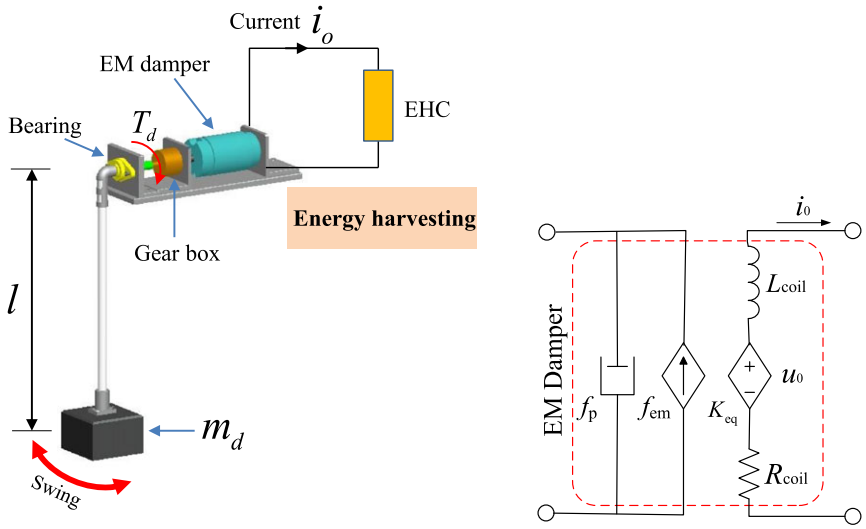

(a) Configuration of pendulum-type TMD (b) Two-port model of EM damper

FIGURE 1 (a) Configuration of pendulum-type energy regenerative tuned mass damper. (b) Two-port model of electromagnetic (EM) damper. EHC, energy-harvesting circuit

3 | CHARACTERIZATION AND MODELING OF ENERGY REGENERATIVE TMD

3.1 | Modeling of EM damper

Energy regenerative TMD is a passive vibration control device. Its frequency is tuned by the length of the pendulum, and its damping is provided by a rotary EM damper and a gear box (as shown in Figure 1(a)). When driven by the pendulum swing, the rotary EM damper generates voltage waveforms, and electric energy is delivered to the EHC attached to the damper. The back electromotive force (emf; i.e., open-circuit voltage) of the EM damper is given by

$$u_o = n_g K_{em} \omega, \tag{1}$$

where n_g is the ratio of the gear box, K_{em} is the motor constant of the EM damper (unit V·s/rad or N·m/A), and ω is the rotational velocity of the EM damper (unit rad/s). According to Lorentz′s law, the back emf produces a current if the circuit is closed. Thus, an EM torque T_{em} is exerted on the oscillating pendulum

$$T_{em} = n_g K_{em} i_0, \tag{2}$$

where i_0 is the instantaneous current in the coils. In addition to the EM torque, parasitic torque exists in the rotary EM damper. Consequently, the total torque is given by

$$T_d = T_p + T_{em} = T_{pt} + C_{pt}\omega + T_{em}, \tag{3}$$

where T_p is the parasitic torque that is assumed to consist of two parts—constant friction torque T_{pt} and viscous damping torque $C_{pt}\omega$—and C_{pt} is the viscous damping coefficient.

If the swing angle θ is small, the pendulum-type TMD can be simplified as a linear-motion TMD, and the corresponding translational velocity and force are given by

$$\dot{z} \approx \omega l, \tag{4}$$

$$f_d = T_d/l, \quad f_p = T_p/l, \quad f_{pt} = T_{pt}/l, \quad f_{em} = T_{em}/l, \tag{5}$$

where $\dot{z}$ is the translational velocity of the TMD relative to the primary structure, l is the length of the pendulum, and f_d, f_p, f_{pt}, and f_{em} are the translational damping force components. On the basis of Equations 1 to 5, the open-circuit voltage and EM damping force of the TMD are given by[17]

$$u_0 = K_{eq}\dot{z}, \quad f_{em} = K_{eq} i_0, \quad K_{eq} = \frac{n_g K_{em}}{l}, \tag{6}$$

where K_{eq} is the equivalent EM motor constant corresponding to the linear motion (unit V·s/m or N/A). Thus, the EM force–velocity ($f_{em} - \dot{z}$) relationship is essentially governed by the voltage–current (u_0–i_0) relationship. Considering the low vibration frequency of civil structures, the inductance of the EM damper can typically be ignored.[27] If the EHC connected to the EM damper is a nearly resistive circuit, the EM damping force f_{em} is proportional to the translational velocity $\dot{z}$, and the corresponding equivalent EM damping coefficient is given by[28]

$$C_{em} = \frac{K_{eq}^2}{R_{coil} + R_{in}}, \tag{7}$$

where R_{coil} is the resistance of the damper coil and R_{in} is the input resistance of the EHC.

The equivalent parasitic damping coefficient C_p (unit N·s/m) corresponding to the linear motion can be calculated by

$$C_p = \frac{f_p}{\dot{z}} = \frac{2T_{pt}}{\pi^2 f d_m l} + \frac{C_{pt}}{l^2}, \tag{8}$$

where d_m is the vibration amplitude of the EM damper and f is the harmonic vibration frequency.

The total equivalent damping coefficient C_d of the EM damper is the superposition of the equivalent EM damping coefficient and the equivalent parasitic damping coefficient[27]:

$$C_d = C_p + C_{em}. \tag{9}$$

A small-scale rotary EM damper was tested in a laboratory. The rotary EM damper is essentially a conventional three-phase alternator that is composed of pairs of permanent magnets and coils. The damper has a length of 94 mm and a diameter of 78 mm. K_{em} was identified as 0.79 V·s/rad according to Equation 1. The measured coil resistance R_{coil} is 34.0 Ω. A gearbox with a ratio of 1:8 was used to enhance the rotational speed of the EM damper. As a result, it also magnified the damping of the EM damper by 64 times.

The rotary EM damper connected to a gearbox was driven by a drilling machine, and the reaction torque was measured by a torsionmeter in laboratory. When the rotary EM damper was not connected to any EHC, the parasitic torque of the rotary EM damper was measured at different rotational velocities. Figure 2 shows the variation in parasitic torque with rotational velocity, which validates the modeling of parasitic damping in Equation 3. The constant parasitic torque T_{pt} and the viscous damping coefficient (C_{pt}) were identified as 0.63 N·m and 0.015 N·ms/rad, respectively, through linear regression shown in Figure 2. Considering a pendulum length of 186 mm, the equivalent machine constant (K_{eq}) is 34.0 Vs/m or N/A according to Equation 6, the equivalent Coulomb force (F_c) is 3.39 N, and the viscous damping coefficient of the parasitic damping C_m corresponding to translational motion is 0.43 N·s/m. The EM damper can be represented by a two-port model shown in Figure 1(b), and its numerical model was established using the Simulink toolbox in the Matlab software, as shown by the EM damper block in Figure 3.

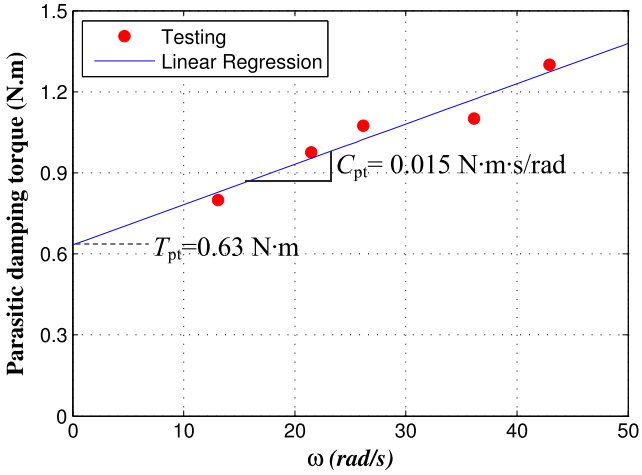

FIGURE 2 Parasitic torque varies with rotational velocity

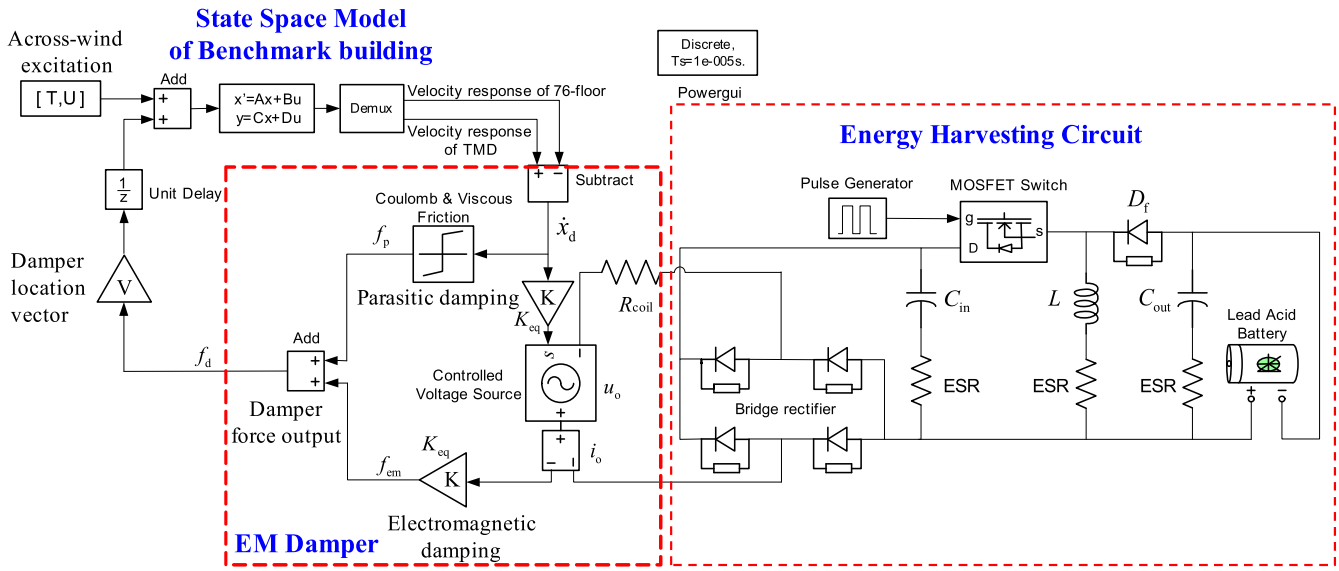

FIGURE 3 Simulink model of the 76-story benchmark building with energy regenerative tuned mass damper (TMD). EM, electromagnetic; MOSFET, metal–oxide–semiconductor field-effect transistor

3.2 | Energy-harvesting circuit

3.2.1 | Principle

When an EHC is connected in an energy regenerative TMD, the electric impedance of the EHC determines the EM damping coefficient according to Equation 7. Therefore, the characteristics of EHC affect both energy-harvesting efficiency and vibration damping performance of the energy regenerative TMD. A variety of EHCs have been developed in the field of power electronics.[42,43] Szarka et al.[43] conducted a comprehensive review of EHC for kinetic energy harvesters. Resistance emulation,[44,45] resistive impedance matching,[46] complex impedance matching,[43] and maximum power point tracking using feedback loop[47,48] are four approaches commonly adopted to achieve optimal energy-harvesting performance. Among them, the resistance emulation is a simple and effective technique to achieve the optimum resistance for the maximal energy-harvesting efficiency[41] and for the optimal damping coefficient according to Equation 7.

In this study, a fixed duty-cycle buck-boost converter (i.e., a resistance emulator)[44] is employed as the EHC for an energy regenerative TMD because of its constant input resistance when operating in discontinuous conduction mode (DCM). Figure 4(a) shows the adopted EHC that consists of a bridge rectifier, a fixed duty-cycle buck-boost converter, and a rechargeable battery. First, the AC voltage generated by the EM damper is converted into DC voltage by the bridge rectifier. The bridge rectifier uses Schottky diodes because of their low forward voltage drop. An input capacitor (C_{in}) connected to the bridge rectifier is used to smooth the DC voltage waveform before inputting to the buck-boost converter. The buck-boost converter behaves similar to a resistor when operated in DCM without any feedback loop and external power supply. The condition for the DCM operation of the fixed duty-cycle buck-boost converter shown in Figure 4(a) is given by[44]

$$U_{\text{rect}} < \frac{1-d}{d} U_{\text{bat}}, \tag{10}$$

where U_{rect}, U_{bat}, and d are the rectifier output voltage, battery voltage, and duty cycle, respectively. If the semiconductors are assumed ideal and the voltage ripple of U_{rect} is ignored, the average input resistance of EHC is given by[42,44]

$$R_{\text{in,dcm}} = \frac{2Lf_{\text{sw}}}{d^2}, \tag{11}$$

where L and f_{sw} are the inductance and the switching frequency of the buck-boost converter, respectively. If the open-circuit voltage $u_0 \gg V_F$, the forward voltage drop effect of the rectifier can be ignored. Thus, Equation 11 provides the

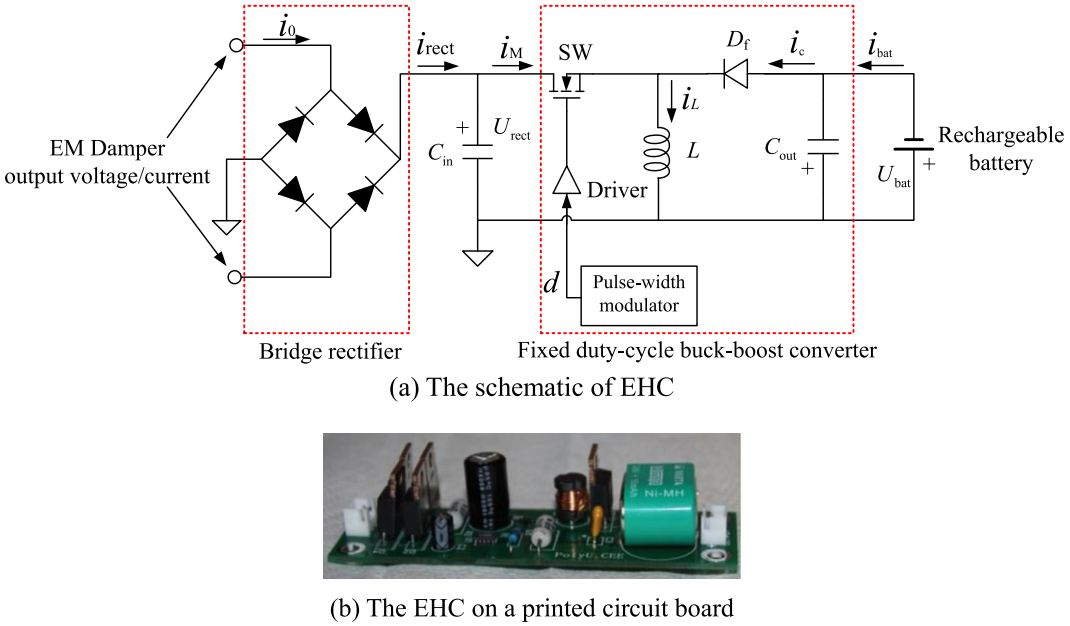

FIGURE 4 Energy-harvesting circuit (EHC). (a) The schematic of EHC. (b) The EHC on a printed circuit board. EM, electromagnetic

equivalent load resistance of EHC. When operating in DCM with a fixed duty cycle, the equivalent load resistance can be maintained nearly constant.

However, if the condition defined by Equation 10 is violated, the DCM operation would transfer to the continuous conduction mode (CCM) operation. As a result, the optimal input resistance in DCM operation could not be maintained in CCM, which leads to possible performance degradation. For example, the EM damping coefficient would increase with increasing power input. This fact implies that the optimum design of energy regenerative TMD would only work in a specific wind speed range depending on the input power or rectifier output voltage level.

3.2.2 | Testing

A small-scale prototype EHC was designed, fabricated, and tested. Figure 4(b) shows the printed circuit board (PCB) of the small-scale prototype EHC, whose size is 3.0 cm × 9.5 cm. In this circuit, a low-power clock oscillator IC (OV-1564-C2, Micro Crystal, Switzerland) with a typical supply voltage in the range of 1.2 to 5.5 V was used to generate a fixed-frequency (f_{sw} = 32.768 kHz) rectangular driving signal for the metal–oxide–semiconductor field-effect transistor (MOSFET, model no. FDV303N). The duty cycle d of the clock oscillator IC is approximately 0.5. Two parallel electrolytic capacitors (680 and 47 μF) were connected to the rectifier output port to smooth the fluctuating waveforms and to store energy to power the clock oscillator IC. Consequently, the clock oscillator IC was powered by the output electric energy from the EM damper. This self-powered feature made the energy regenerative TMD a more feasible standalone system. A rechargeable NiMH battery (nominal voltage 3.7 V) was used because of its low charging current that ranges from 8.4 to 140 mA. An additional 10-μF tantalum capacitor was added parallel to the NiMH battery to reduce ripple current across the battery, thus prolonging battery life. All the diodes were Schottky diodes with a forward voltage drop V_F of only 0.22 V. On the basis of the typical duty cycle (d = 0.5) and switching frequency f_{sw} = 32.768 kHz, an inductor (L = 68 μH) was used to emulate a 17.8-Ω resistor according to Equation 11. The fixed duty-cycle buck-boost converter operates in DCM on the theoretical condition (Equation 10) that the rectifier output voltage is less than 5.1 V.

The input resistance and efficiency of the PCB were experimentally characterized. A DC power supply (model NP-9615) was used to simulate the input power to the PCB. The output signal of the clock oscillator IC and the driving signal for the MOSFET were measured by an Agilent oscilloscope (model Agilent DSO1024A). The rectifier output current and the charging current were measured through the voltage drop of two 0.05-Ω high-precision resistors, where small voltage drop signals were amplified by the voltage amplifier and filter (model SR640 dual-channel filters) with an amplification factor of 40 dB. All signals of interest, including the rectifier output voltage and NiMH battery voltage, were collected by using a Kyowa EDX-100A data acquisition system with a sampling frequency of 500 Hz. A low-pass analog filter was set with a cut-off frequency of 100 Hz.

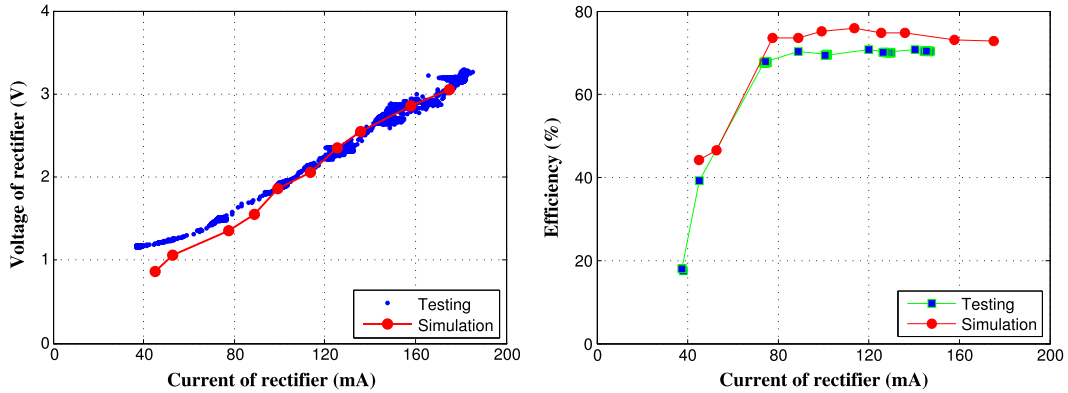

(a) Voltage–current relationship of rectifier output port (b) Efficiency-current curve of EHC

FIGURE 5 Comparison of measured and numerical results of energy-harvesting circuit (EHC). (a) Voltage–current relationship of rectifier output port. (b) Efficiency–current curve of EHC.

Figure 5(a) shows the voltage–current relationship (i.e., u_{rect}–i_{rect} relationship) of the rectifier output port, which characterizes the input impedance of the EHC. The rectifier output current i_{rect} linearly rises with increasing rectifier output voltage u_{rect} when the rectifier voltage is larger than 1.3 V, whereas a linear relationship with a smaller slope was observed when the rectifier voltage is smaller than 1.3 V. The approximately linear u_{rect}–i_{rect} relationship implies that the input impedance of the DCM buck-boost converter is nearly resistive. Thus, Figure 5(a) provides evidence that the adopted EHC can approximately emulate a constant resistor. The average input resistance was estimated to be 18.4 Ω. This value is very close to the theoretical prediction (17.8 Ω) given by Equation 11 with duty cycle $d = 0.5$.

Figure 5(b) shows that the efficiency varies with the rectifier current. The EHC efficiency rapidly increases from 18% to 68% when i_{rect} varies from 38 to 75 mA. The value then becomes approximately constant (71%). The variation may be attributed to the change law of on-resistance R_{on} of the MOSFET. The on-resistance R_{on} in the small-scale prototype EHC may be up to several ohms during low-current operation (<75 mA) but is close to the typical value (0.33 Ω) during high-current operation (>75 mA). Therefore, a low on-resistance feature of the MOSFET is important in EHC design.

3.2.3 | Modeling

The EHC was simulated using the SimPowerSystems toolbox in Matlab Simulink environment. The corresponding Simulink model for the EHC is shown as one block of Figure 3. The values of electronic components were set in accordance with the circuit design. The simulation results were compared with the experimental results. As shown in Figure 5(a), the numerical voltage–current curve of EHC is close to the measured one, which verifies the validity of the Simulink model of the EHC. In addition, the peak circuit efficiency predicted by the simulation is approximately 74% when the current is larger than 70 mA, as shown in Figure 5(b), which is slightly higher than the measured efficiency within this current range. During low-current operation ($i_{\text{rect}} < 75$ mA), the on-resistance R_{on} of the MOSFET is equal to 6 Ω, which is significantly larger than the typical value (0.33 Ω). In this low-current range, the numerical results can fairly match the experimental results. As the power/current of EHC in real applications of an energy regenerative TMD in building structures is much higher than that in the small-scale test, the R_{on} of the MOSFET would be close to its typical value. In general, the Simulink model shows good agreement with the performance of the tested EHC.

3.3 | Modeling of pendulum-type energy regenerative TMD

Figure 6 shows a small-scale pendulum-type energy regenerative TMD fabricated using the tested rotary EM damper described in Section 3.1. The parameters of the energy regenerative TMD are presented in Table 1. The rotary EM damper was connected to a three-phase rectifier and a constant resistor ($R_{\text{load}} = 100$ Ω), because the fixed duty-cycle buck-boost converter when operated in DCM can be approximately represented by a constant resistor. Free-vibration tests were conducted. Displacement response was collected using a Kyowa EDX-100A data acquisition system with a sampling frequency of 1000 Hz, and the voltage of the constant resistor was measured using an oscilloscope (model Tektronix TDS 224).

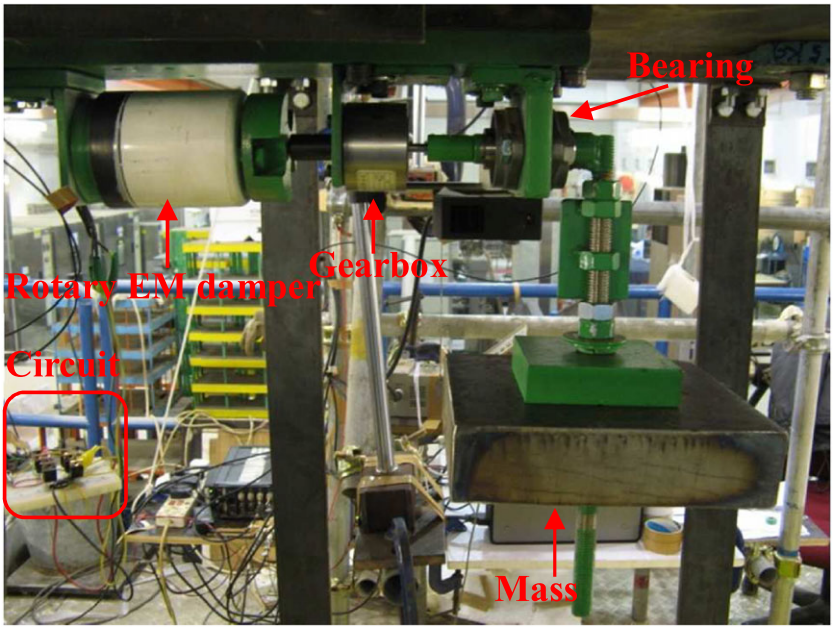

FIGURE 6 Experimental setup of a small-scale pendulum-type energy regenerative tuned mass damper. EM, electromagnetic

TABLE 1 Parameters of small-scale pendulum-type energy regenerative tuned mass damper (TMD)

Parameter	Value	Parameter	Value
Machine constant, K_{em} (Vs/rad or Nm/A)	0.79	Mass of TMD, m (kg)	17.6
Coil resistance, R_{coil} (Ω)	34.0	Length of pendulum, l (mm)	186
Gearbox ratio, n_g	8	Frequency of TMD, f_{tmd} (Hz)	1.06
Constant parasitic torque (Nm)	0.63	Equivalent machine constant, K_{eq} (Vs/m or N/A)	34.0
Parasitic damping coefficient, C_{pt} (Nms/rad)	0.015		

On the basis of the model of the EM damper and EHC, a Simulink model of the small-scale pendulum-type TMD was built by incorporating the TMD parameters (including the mass and stiffness of the pendulum-type TMD). The numerical model is consistent with the experimental model, and the corresponding parameters of the Simulink model are set in accordance with those shown in Table 1.

The dynamic simulation was performed with a time step of 1 ms. Figure 7(a) shows a comparison of the measured and numerical free-vibration translational displacement of the energy regenerative TMD. Figure 7(b) shows the time

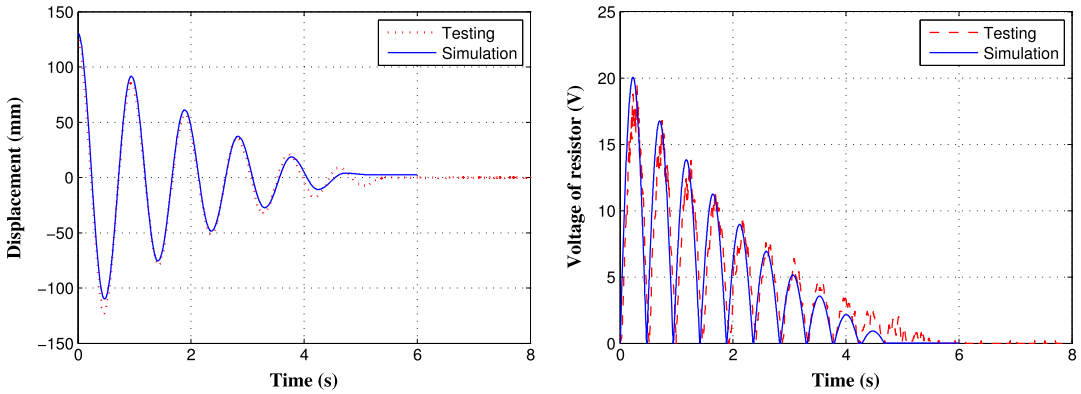

(a) Translational displacement (b) Voltage of resistor

FIGURE 7 Comparison of measured and numerical results in small-scale pendulum-type energy regenerative tuned mass damper free-vibration case (R_{load} = 100 Ω). (a) Translational displacement. (b) Voltage of resistor

history of voltage of the constant resistor during the free vibration. Generally good agreement is found between the measured and numerical results; this finding demonstrates the accuracy of simulation using the established Simulink model.

Consequently, an energy regenerative TMD can be well simulated using the Simulink model by integrating the EM damper, pendulum-type TMD, and EHC modules described in Section 3. It enables the performance assessment of an energy regenerative TMD in full-scale high-rise buildings.

4 | OPTIMAL DESIGN OF ENERGY REGENERATIVE TMD

The design of an energy regenerative TMD should consider both vibration mitigation and energy-harvesting performance. The resistance emulation feature of the buck-boost converter makes the EM damping nearly linear if the EHC is operated in DCM. The nonlinear parasitic damping can be linearized using Equation 8. The dynamics of the energy regenerative TMD can be approximated by a passive TMD.[7] Therefore, the optimal tuning laws obtained by Den Hartog can be applied in this study,[1]

$$\gamma_{\text{opt}} = \frac{1}{1+\mu}, \tag{12}$$

$$\zeta_{\text{opt}} = \sqrt{\frac{3\mu}{8(1+\mu)}}, \tag{13}$$

where γ_{opt} and ζ_{opt} are the optimal frequency ratio and damping ratio of the energy regenerative TMD, respectively; and $\mu = m_{\text{d}}/m_{\text{s}}$ is the ratio of the TMD mass to the structural mass. For a multi-DOF (MDOF) structure–TMD system, the above equations can still be applied by considering modal mass and modal stiffness.[5,7]

The optimal frequency ratio is fulfilled by tuning the length of the pendulum, whereas the optimal damping ratio is tuned by setting a target EM damping coefficient given by

$$C_{\text{em,opt}} = 2m_{\text{d}}\omega_{\text{d}}\zeta_{\text{opt}} - C_{\text{p}}, \tag{14}$$

where ω_{d} is the natural circular frequency of the energy regenerative TMD. The optimal EM damping coefficient is actually amplitude dependent because of the coulomb friction effect in C_{p}, and thus the optimal design requires an approximate evaluation of vibration amplitude. Given the target EM damping coefficient, the corresponding optimal input resistance of EHC with respect to vibration control performance can be estimated according to Equation 7.

$$R_{\text{opt,C}} = \frac{K_{\text{eq}}^2}{C_{\text{em,opt}}} - R_{\text{coil}}. \tag{15}$$

On the other hand, energy-harvesting efficiency needs to be maximized. The energy-harvesting efficiency η is the product of three energy conversion coefficients[27]:

$$\eta = \frac{P_{\text{out}}}{P_{\text{in}}} = \eta_1\eta_2\eta_3, \tag{16a}$$

$$\eta_1 = C_{\text{em}}/\left(C_{\text{em}} + C_{\text{p}}\right), \tag{16b}$$

$$\eta_2 = R_{\text{in}}/(R_{\text{in}} + R_{\text{coil}}), \tag{16c}$$

where P_{out} and P_{in} are the effective output power and damping power of energy regenerative TMD, respectively; η_1 is the electromechanical coupling coefficient; η_2 is the ratio of gross output power to EM damping power; and η_3 is the efficiency of EHC (i.e., the fixed duty-cycle buck-boost converter). High electromechanical coupling always benefits energy harvesting. The electromechanical coupling coefficient η_1 is affected by the equivalent parasitic damping coefficient C_{p} and the EM damping coefficient C_{em}. It was found that a small parasitic damping C_{p} or a high equivalent

machine constant K_{eq} can maximize the electromechanical coupling coefficient.[27] According to Equation 16c, a small resistance of the damper coil R_{coil} benefits the energy conversion coefficient η_2. To achieve the maximum energy-harvesting efficiency, the optimal input resistance of EHC is given as follows[27]:

$$R_{opt,E} = R_{coil}\sqrt{1 + \frac{K_{eq}^2}{C_p R_{coil}}}\ . \tag{17}$$

Accordingly, the theoretical maximum harvesting efficiency reads as follows:

$$\eta_{max} = \frac{K_{eq}^2 \alpha_{opt}}{C_p R_{coil}\left(1+\alpha_{opt}\right)^2 + K_{eq}^2\left(1+\alpha_{opt}\right)}, \tag{18}$$

where $\alpha_{opt} = R_{opt\,,\,E}/R_{coil}$.

An optimal design of the dual-function energy regenerative TMD requires the input resistance of EHC satisfy both Equations 15 and 17 simultaneously. Consequently, the parameters K_{eq}, C_p, and R_{coil} of the EM damper have to be properly designed, implying that the EM damper should be tailor-made. If the optimal input resistance of EHC is determined, the parameters of the DCM buck-boost converter, including the switching frequency f_{sw}, inductance L, and the duty cycle d, are subsequently calculated according to Equation 11. If a trade-off must be made between vibration control and energy-harvesting performance, the optimal damping coefficient should be first fulfilled in the design of an energy regenerative TMD. The effectiveness of the proposed simple optimal design approach for the energy regenerative TMD will be carefully examined in the full-scale numerical study in next section.

5 | FULL-SCALE NUMERICAL STUDY

A numerical study was conducted to investigate the performance of the energy regenerative TMD in a benchmark building that represents a full-scale, 76-story, 306-m-high building subjected to across-wind excitation. The numerical study was implemented in Matlab Simulink environment as well. The results of the numerical simulations with respect to vibration control performance and energy-harvesting efficiency are presented in this section.

5.1 | Wind-excited 76-story benchmark building

A control benchmark problem of a 76-story building was established by Yang et al.[49] All the codes and data could be downloaded from the corresponding website. The 76-story, 306-m-high building with a height-to-width ratio of 7.3 represents a typical wind-sensitive tall building. The across-wind force time histories were determined through a wind tunnel test of a 1:400 scale model with a velocity scale approximately equal to 1:3.[50] Wind data were recorded over a total of 27 s in the wind tunnel test, which approximately corresponded to an hour of wind data for the full-scale building in accordance with a time scale of 1:133. All the recorded pressure coefficients were converted to the across-wind force time histories acting on the 76 DOFs of the benchmark building model under a mean wind speed of 47.25 m/s at the top of the building. These wind force data were scaled by a factor of $(U_h/47.25)^2$ to represent other mean wind speed U_h at the top of the benchmark building (i.e., 306 m high).[49,50] In wind force generation, the mean wind speed $\overline{U}_r$ at the height of 10 m above the ground was first assumed. Then, the mean wind speed U at the top of the building was determined according to a power law. Finally, the wind force time histories were determined on the basis of the scaling factor $(U/47.25)^2$.

5.2 | Application of energy regenerative TMD to benchmark building

In this numerical study, an energy regenerative TMD building was first designed for the 76-story wind-excited benchmark building. A 500-ton TMD, which corresponds to a mass ratio of 1.33%, was installed at the top floor. The TMD was intended to suppress the first modal responses of the benchmark building. Therefore, the optimal frequency and damping ratios of the energy regenerative TMD were determined according to Equations 12 and 13, as shown in Table 2. The target damping coefficient C_{opt} of the energy regenerative TMD is 69.54 kN·s/m, which corresponds to the optimal damping ratio of TMD.

The damping and energy-harvesting performance of the energy regenerative TMD are dependent on both the EM damper and EHC. An EM damper (K_{eq} = 939.5 V·s/m, R_{coil} = 4.8 Ω, F_c = 0.5 kN, C_m = 14.4 kN·s/m) was assumed to be used in this numerical study. The parasitic damping coefficient C_p is dependent on vibration frequency and amplitude because of the presence of coulomb friction force. In this study, an equivalent parasitic damping coefficient C_p was evaluated before the design of EHC on the basis of the optimal frequency of the TMD (i.e., 0.158 Hz) and the estimated average vibration amplitude (67 mm) within the mean wind speed range of 4 to 14 m/s. As a result, the estimated parasitic damping coefficient C_p was calculated to be 24.0 kN·s/m using Equation 8. To achieve maximum harvesting efficiency, the target input resistance R_{in} of the EHC was subsequently determined to be 14.1 Ω using Equation 17. The resultant total damping coefficient C_d is 70.6 kN·s/m, which is close to the optimal damping coefficient C_{opt} of TMD.

A lead acid rechargeable battery (nominal voltage of 216 V; capacity of 20 Ah) was employed as the energy storage element. The EHC design considers the practical parameters of the electronic components. The on-resistance R_{on} and equivalent series resistance (ESR) of the MOSFET and the ESR of the inductor and capacitor are shown in Table 3 on the basis of the component datasheet.

Figure 3 shows the Simulink block of the benchmark building installed with the energy regenerative TMD. A state space model represents a 77-DOF model considering the 76-story benchmark building and the energy regenerative TMD. The EHC was directly built in the Matlab/SimPowerSystems environment. The diodes, MOSFET, rechargeable battery, inductor, and capacitors were properly modeled. The electronic models consider detailed parameters, such as forward voltage drop V_F, ESR, on-resistance R_{on} of MOSFET, and internal diode resistance R_d of MOSFET, to simulate the practical behaviors of the devices. The wind loads were scaled depending on different mean wind speeds.[49,50] The EM damper block and the EHC block were integrated into the Simulink model to conduct the coupled dynamic analysis. The simulation was performed with a time step of 10 μs during the entire duration of 300 s for each mean wind speed case.

All the currents and voltages of the circuit were recorded with a sampling frequency of 100 Hz. The structural responses under wind loads were also output for vibration control performance evaluation. The control effect was

TABLE 2 Parameters of the energy regenerative tuned mass damper (TMD) of the Simulink model in the benchmark simulation

Benchmark building and TMD	Value	EM damper and EHC	Value
First modal mass of building (ton)	37,594	Coulomb friction force, F_c (kN)	0.5
Fundamental frequency of building (Hz)	0.16	Viscous damping coefficient, C_m (kN·s/m)	14.4
Mass of TMD, m_d (ton)	500	C_{em} in DCM (kN·s/m)	46.6
Mass ratio of TMD, μ (%)	1.33	Machine constant, K_{eq} (V·s/m or N/A)	939.5
Frequency ratio of TMD, γ_{opt}	0.987	Resistance of coils, R_{coil} (Ω)	4.8
Frequency of TMD, f_{tmd} (Hz)	0.158	Average input resistance in DCM, R_{in} (Ω)	14.1
Damping ratio of TMD, ζ_{opt} (%)	7.01		
C_{opt} (kN·s/m)	69.54		

Note. DCM = discontinuous conduction mode; EHC = energy-harvesting circuit; EM = electromagnetic.

TABLE 3 Parameters of energy-harvesting circuit in the benchmark simulation

Parameter	Value	Parameter	Value
V_F of diode (V)	0.22	Switch frequency, f_{sw} (kHz)	10
Filter capacitor, C_{in} (μF)	2200	Inductance, L (μH)	112.8
ESR of filter capacitor (mΩ)	11	ESR of inductor (mΩ)	200
R_{on} of MOSFET (mΩ)	200	Output capacitor, C_{out} (μF)	1200
R_d of MOSFET (mΩ)	10	ESR of output capacitor (mΩ)	18
Duty cycle of buck boost (%)	40	Output voltage of buck boost (V)	216

Note. MOSFET = metal–oxide–semiconductor field-effect transistor.

evaluated by using the following performance criteria[49]:

$$J_1 = \max(\sigma_{\ddot{x}_i})/\sigma_{\ddot{x}_{75o}}, \quad J_3 = \sigma_{x_{76}}/\sigma_{x_{76o}}, \quad J_7 = \max(\ddot{x}_{pi})/\ddot{x}_{p75o}, \quad J_9 = x_{p76}/x_{p76o}, \tag{19}$$

where $\sigma_{\ddot{x}_i}$ is the root mean square (RMS) acceleration of the ith floor (i = 1, 30, 50, 55, 60, 65, 70, 75) with control (i.e., with the energy regenerative TMD); $\sigma_{\ddot{x}_{75o}}$ is the RMS acceleration of the 75th floor without control; $\sigma_{x_{76}}$ and $\sigma_{x_{76o}}$ are the RMS displacements of the 76th floor with control and without control, respectively; $\ddot{x}_{p_i}$ is the peak acceleration of the ith floor with control; $\ddot{x}_{p_{75o}}$ is the peak acceleration of the 75th floor without control; and x_{p76} and x_{76o} are the peak displacement responses of the 76th floor with control and without control, respectively.

5.3 | Numerical results

This section presents the numerical results of the full-scale 76-story wind-excited benchmark building equipped with the energy regenerative TMD with respect to circuit characteristics, vibration control performance, and energy-harvesting performance.

5.3.1 | Circuit characteristics

Figure 8(a) shows the voltages of the rectifier output port U_{rect}, including the peak and mean voltages, under different wind speeds. When the mean wind speed changes from 4 to 25 m/s, the mean voltage of the rectifier output port varies from 10.8 to 280.5 V, whereas the peak voltage varies from 35.4 to 676.9 V. The switching frequency of the converter (10 kHz) is considerably higher than that of structural responses (f_1 = 0.158 Hz). Thus, the converter would respond quickly to the transient voltage of the rectifier output port. As indicated by Equation 10, the operation mode of the buck-boost converter of EHC depends on the rectifier output voltage: The buck-boost converter operates in DCM when the rectifier voltage U_{rect} is below the threshold voltage of 324 V and in CCM when U_{rect} is higher than the threshold. As shown in Figure 8(b), the EHC always operates in DCM under the mean wind speed of 4 to 12 m/s. When the mean wind speed is above 12 m/s, the buck-boost converter partially operates in CCM. However, its operation is still mostly dominated by DCM. For example, the buck-boost converter operates in DCM 90.1% of time under the mean wind speed of 16 m/s.

The percentage of time between DCM and CCM operation modes affects the equivalent input resistance of EHC, R_{in}. Such a variation in R_{in} may affect both the vibration control and the energy-harvesting performance in terms of EM damping, output power, and efficiency. Figure 9 shows the variation of equivalent input resistance under different wind speeds. As explained in Section 3.2.1, CCM leads to the decrease in the input resistance. Conversely, a too low rectifier voltage U_{rect} increases the input resistance because the buck-boost converter cannot efficiently work in this case. As a result, the average input resistance of the circuit is close to the target optimal resistance (14.1 Ω) between the mean wind speeds of 7 and 16 m/s.

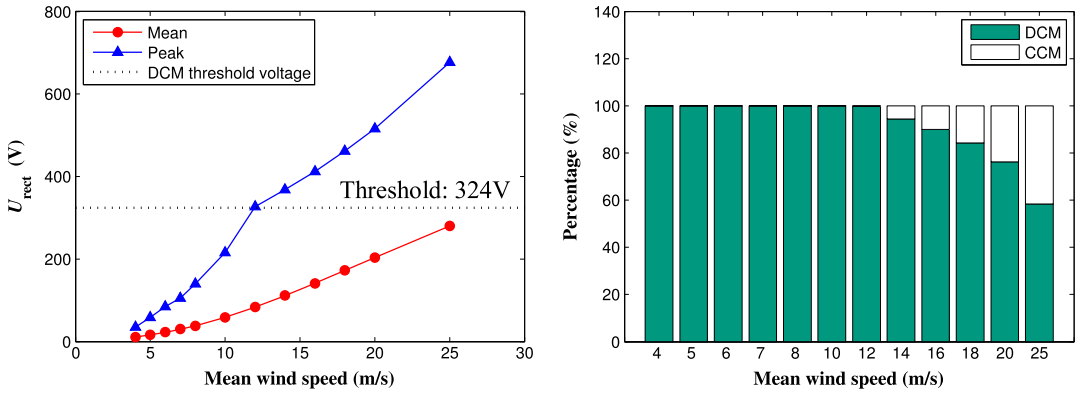

(a)Voltage of rectifier output port (b) Percentage of DCM/CCM operation

FIGURE 8 Peak/root mean square (RMS) voltage of rectifier output port and percentage of discontinuous conduction mode/continuous conduction mode (DCM/CCM) operation. (a) Voltage of rectifier output port. (b) Percentage of DCM/CCM operation

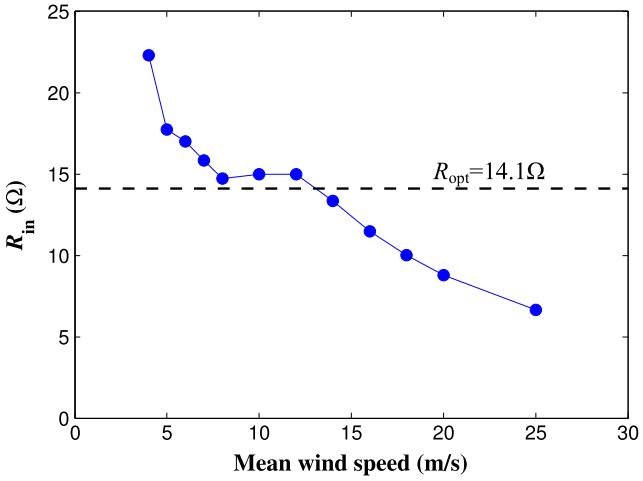

FIGURE 9 Average input resistance of energy-harvesting circuit varies with mean wind speed

5.3.2 | Vibration control performance

Similar to the conventional TMD, the energy regenerative TMD is essentially a passive control device. However, its damping coefficient may vary under different vibration levels. Figure 10 shows the variations in the parasitic, EM, and total damping coefficients of the EM damper with increasing mean wind speed. The equivalent parasitic damping coefficient decreases with increasing vibration amplitude because of the existence of coulomb damping force (Equation 8). On the one hand, the parasitic damping coefficient C_p rapidly declines in the mean wind speed range of 4 to 10 m/s and becomes relatively stable with the further increase in mean wind speed. On the other hand, the EM damping coefficient C_{em} changes with the average input resistance of EHC. Within the wind speed range of 7 to 12 m/s, the buck-boost converter of EHC operates completely in DCM; thus, the average input resistance of the circuit and the resultant EM damping coefficient remain approximately constant. If the mean wind speed exceeds 12 m/s, the buck-boost converter partially operates in CCM, which decreases the average input resistance and increases the EM damping.

The total damping coefficient of the energy regenerative TMD, C_d, is the sum of equivalent parasitic damping C_p and EM damping C_{em}. In a wide mean wind speed range of 7 to 16 m/s, the total damping coefficient C_d of the energy regenerative TMD varies from 63.4 to 71.2 kN·s/m, which is close to the optimum value of 69.54 kN·s/m. Notably, the increment of EM damping is partially compensated by the decrement in parasitic damping. As a result, the total damping coefficient C_d is still near the optimum value when the mean wind speed exceeds 16 m/s.

Figure 11 shows the control performance for the energy regenerative TMD and the optimally designed conventional TMD, where the performance indexes are defined by Equation 19. In general, the energy regenerative TMD achieves

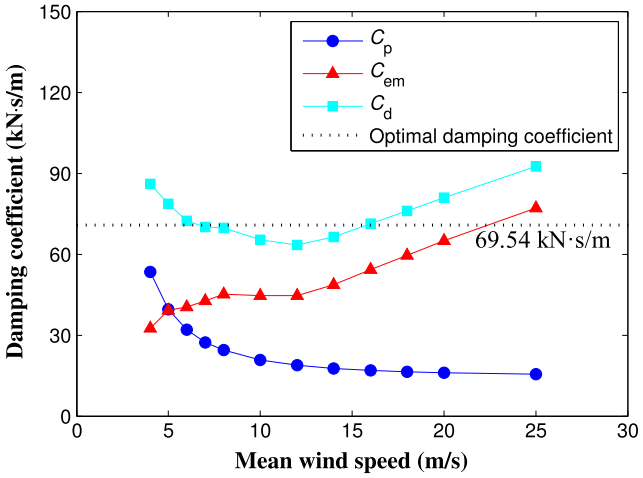

FIGURE 10 Damping coefficients varies with mean wind speed

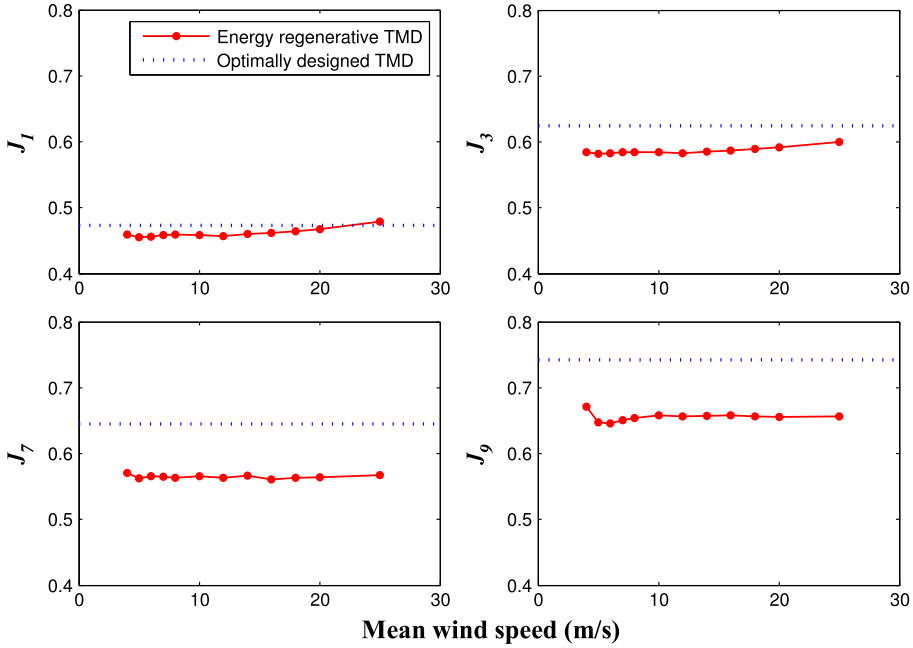

FIGURE 11 Control performance indexes vary with mean wind speed. TMD, tuned mass damper

slightly better vibration suppression performance than does the optimally designed TMD with only viscous damping (except J_1 at 25 m/s). This interesting phenomenon may be attributed to the positive effect of friction in the large amplitude vibration of TMD. Figure 11 indicates that the control performance of the energy regenerative TMD is generally insensitive to the variation of its total damping ratio. For example, the damping ratio of regenerative TMD connected to the EHC varies from 6.4% to 9.33% when the mean wind speed increases from 4 to 25 m/s; however, the variation in the control performance index is less than 4%. Even though the total damping coefficient C_d is 33.1% more than the optimum setting at the mean wind speed of 25 m/s, the energy regenerative TMD maintains good vibration control performance, which validates the conclusion that the control performance of TMD is insensitive to damping detuning.[5]

Figure 12 shows the acceleration responses of the building at the wind speed of 12 m/s, where Figure 12(a) shows the acceleration time history of the top floor (76th floor) and Figure 12(b) shows the distribution of RMS acceleration heightwise direction. The peak acceleration responses of the top floor are reduced by 33.4% and 35.5%, respectively, by the optimally designed conventional TMD and the energy regenerative TMD. The RMS acceleration responses are reduced by approximately 52.8% by both the optimally designed conventional TMD and energy regenerative TMD. Similar results can be obtained for displacement response, although not shown in the figure. The peak displacements of the

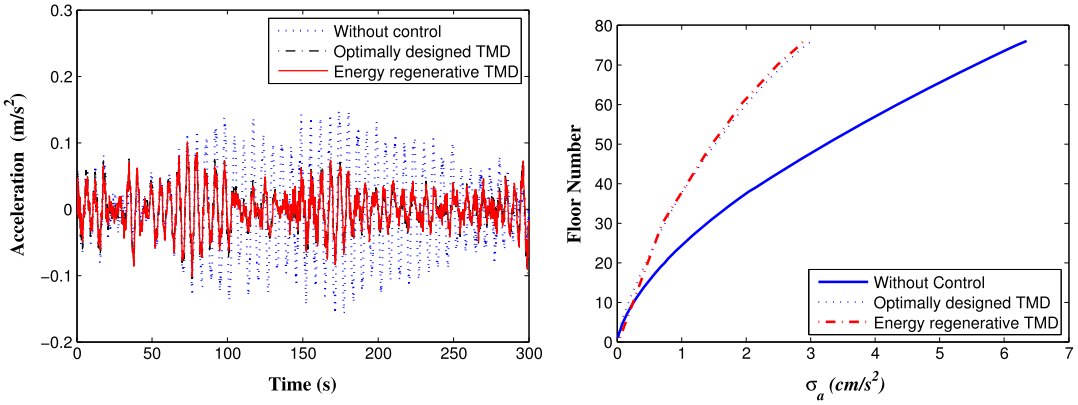

(a) Acceleration time history at the roof (b) RMS acceleration response

FIGURE 12 Structural acceleration responses with and without control (mean wind speed 12 m/s). (a) Acceleration time history at the roof. (b) Root mean square acceleration response. TMD, tuned mass damper

top floor are reduced by 25.7% and 34.4%, respectively, by the conventional TMD and the energy regenerative TMD. The RMS displacement responses are reduced by approximately 40.4% by both TMDs. The overall vibration mitigation performance is close, and the introduction of the energy-harvesting function in the novel energy regenerative TMD does not degrade the vibration control performance in this wind-excited benchmark building problem.

5.3.3 | Energy-harvesting performance

Figure 13(a) shows the effective output power of energy regenerative TMD (i.e., the charging power of the battery) under cross-wind excitation with different mean wind speeds. The cut-in wind speed for electrical power generation is 4 m/s, as shown in Figure 13. Under cross-wind excitations, the energy regenerative TMD generates a large amount of electrical power because of its large mass. The average output power ranges from 2.3 to 60.7 W in the mean wind speed range of 4 to 7 m/s, and then increases to 108.6 to 604.7 W in the mean wind speed range of 8 to 12 m/s. If the mean wind speed is greater than 14 m/s, then the output power from regenerative TMD is up to kilowatts (e.g., 51.7 kW in the extreme wind speed of 40 m/s). The numerical results suggest that the energy regenerative TMD can effectively harvest the vibration energy of high-rise building subjected to across-wind excitation within a wide range of wind speed. Even under a low wind speed, the output power is enough to power a few wireless sensors or alarm devices; under an extreme wind speed (e.g., 25 m/s), the output power is considerably greater and can power a comprehensive structural monitoring system in the same building.

Figure 13(b) shows the energy-harvesting efficiency of energy regenerative TMD with different mean wind speeds. With the increase in vibration amplitudes or mean wind speeds, C_p continuously decreases until an asymptotic value is reached, whereas C_{em} gradually increases with decreasing R_{in} when partially operating in CCM (Figure 8(b)). As a result, η_1 continuously increases with increasing mean wind speed. The efficiency η_2 depends on the average input resistance R_{in} of the EHC. Therefore, the decreasing trend of η_2 with increasing wind speed can be explained by the variation in R_{in} (Figure 9). The average input resistance R_{in} cannot maintain the optimal value when the buck-boost converter of EHC operates partially in CCM; as a result, η_2 decreases when the mean wind speed is greater than 12 m/s. The efficiency of the EHC η_3 mainly depends on the current magnitude that flows through the circuit. η_3 is relatively low in the low mean wind speed of 4 to 5 m/s, but it can maintain a satisfactory efficiency, which ranges from 65.7% to 79.9%, in the wind speed range of 6 to 25 m/s.

Consequently, the overall energy-harvesting efficiency η of the regenerative TMD dramatically increases from 12.8% to 35.9% in the mean wind speed range of 4 to 7 m/s and then retains a high efficiency within the mean wind speed range of 7 to 25 m/s, as shown in Figure 13(b). The overall energy-harvesting efficiency η refers to the ratio of the average output power to the average damping power of the energy regenerative TMD. The majority of the damping power of the regenerative TMD is still dissipated or transferred to heat. Thus, overlooking various types of power loss may significantly overestimate the ultimate output power.

The total input power from wind excitation to the structure is also evaluated in the numerical study. The excitation power is equal to the sum of the damping power of TMD and the inherent damping power of the structure if the structure is subjected to a stationary vibration. Figure 14 shows the distribution of the total excitation power under

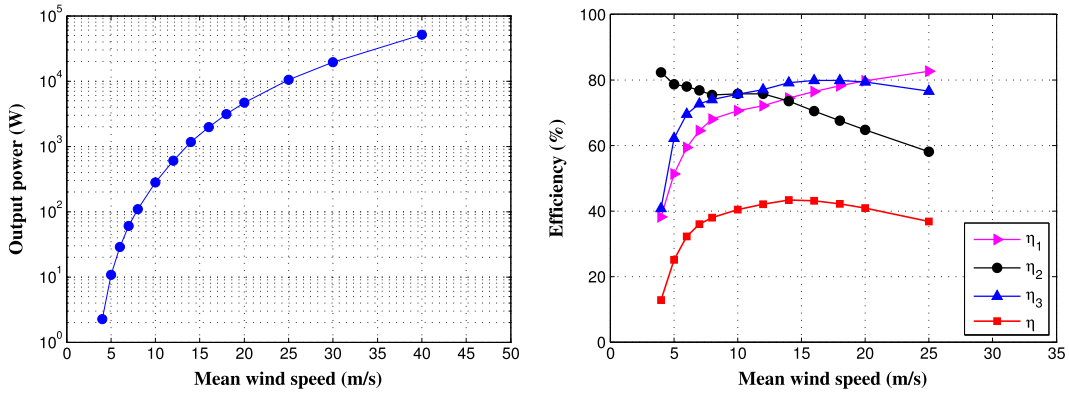

(a) Output power (b) Efficiencies

FIGURE 13 Output power and energy-harvesting efficiencies varies with mean wind speed. (a) Output power. (b) Efficiencies

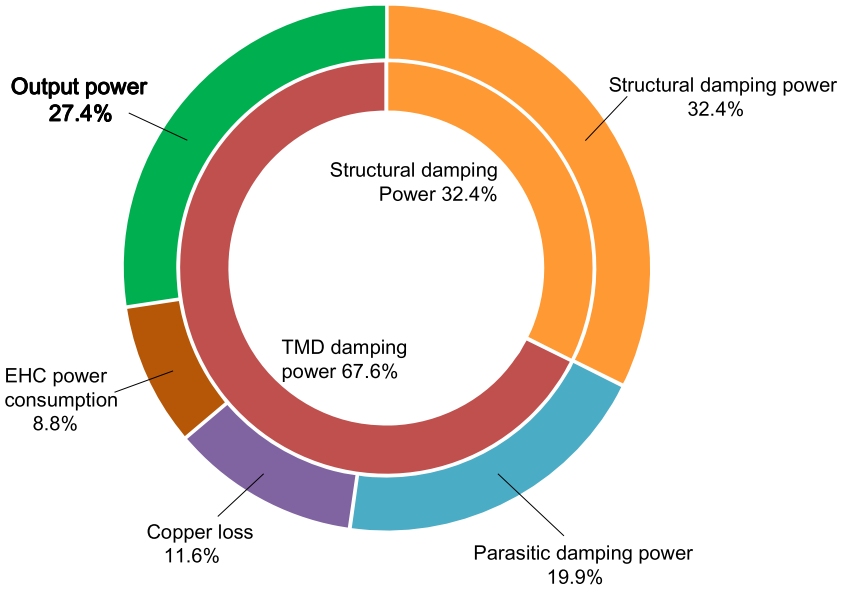

FIGURE 14 Distribution of the total wind excitation power in the benchmark building with the energy regenerative tuned mass damper (TMD) at the mean wind speed of 10 m/s. EHC, energy-harvesting circuit

the mean wind speed of 10 m/s, in which 32.4% is dissipated by the structural inherent damping mechanism, and 27.4% is finally stored in the rechargeable battery via the EHC. Thus, the harvested electrical power is still much less than the total excitation power. The ratio of the TMD damping power can be enhanced by increasing the mass ratio of TMD, that is, the ratio of the TMD mass to the structural mass. However, the mass ratio is typically small due to some practical constraints.

6 | CONCLUSIONS

This paper investigates the feasibility and effectiveness of using energy regenerative TMD in high-rise buildings for simultaneous vibration control and energy harvesting. A comprehensive study on a pendulum-type energy regenerative TMD, including characterization, modeling, optimal design, and full-scale performance evaluation in consideration of the nonlinearities in EM damper and EHC, is conducted. A simple design method for determining the design parameters of the energy regenerative TMD is presented on the basis of the classical optimal TMD tuning law and the optimal resistance matching for maximal energy-harvesting efficiency. The numerical simulation of a full-scale, 76-story, wind-excited benchmark building with the energy regenerative TMD illustrates that the vibration control performance and energy-harvesting efficiency exhibit vibration amplitude dependence. The control effect was found to be insensitive to the slight change in the damping ratio of TMD, and robust vibration control performance comparable to an optimally designed passive TMD is observed within a wide range of wind speed (4 to 25 m/s). Slight deterioration of vibration control performance is also observed at extreme mean wind speed (e.g., 40 m/s), because of damping deviating from its optimal setting. Meanwhile, a great amount of electric power is harvested via the EHC connected to the energy regenerative TMD. The net output power for battery charging is up to hundreds of watts to kilowatt level with very high efficiency (ranging from 37.9% to 43.3%) within the optimal mean wind speed range of 8 to 25 m/s.

The numerical simulation results demonstrate the promising prospect of applying the proposed energy regenerative TMD in real-world building structures. The properly designed energy regenerative TMD achieves the optimal vibration control and energy-harvesting performance in the optimal wind speed range. Notably, the optimal mean wind speed range can be adjusted by changing the EHC design. The improved setting of the optimal wind speed range needs to be investigated in future.

ACKNOWLEDGEMENT

The authors are grateful for the financial support from the Research Grants Council of Hong Kong through a GRF grant (project PolyU 5330/11E), from the National Natural Science Foundation of China (projects 51508217 and 51629801), and from the Hong Kong Polytechnic University (project 1-ZVJS).

REFERENCES

[1] J. P. Den Hartog, *Mechanical vibrations*, McGraw-Hill, New York **1947**.

[2] Y. L. Xu, K. C. S. Kwok, B. Samali, *J. Wind Eng. Ind. Aerodyn.* **1992**, *40*(1), 1.

[3] K. C. S. Kwok, B. Samali, *Eng. Struct.* **1995**, *17*(9), 655.

[4] T. T. Soong, G. F. Dargush, *Passive energy dissipation systems in structural engineering*, John Wiley & Sons, New York, USA **1997**.

[5] R. Rana, T. T. Soong, *Eng. Struct.* **1998**, *20*(3), 193.

[6] C. C. Chang, *Eng. Struct.* **1999**, *21*(5), 454.

[7] J. J. Connor, *Introduction to structural motion control*, Prentice Hall/Pearson Education, Upper Saddle River, USA **2003**.

[8] R. R. Gerges, B. J. Vickery, *Struct. Design Tall Spec. Build.* **2005**, *14*(4), 353.

[9] F. Casciati, F. Giuliano, *J. Vib. Control.* **2009**, *15*(6), 821.

[10] V. B. Patil, R. S. Jangid, *J. Civ. Eng. Manag.* **2011**, *17*(4), 540.

[11] A. Tributsch, C. Adam, *Smart Struct. Syst.* **2012**, *10*(2), 155.

[12] M. G. Soto, H. Adeli, *Arch. Comput. Meth. Eng.* **2013**, *20*(4), 419.

[13] G. L. Lin, C. C. Lin, B. C. Chen, T. T. Soong, *Eng. Struct.* **2015**, *83*, 187.

[14] Zhu S, Shen W, Xu YL. Regenerative electromagnetic TMD—A novel integration of energy harvesting and vibration control, Proceedings of the 6th International Workshop on Advanced Smart Materials and Smart Structures Technology, ANCRiSST2011, Dalian, China, **2011**.

[15] I. L. Cassidy, J. T. Scruggs, S. Behrens, H. P. Gavin, *J. Intell. Mater. Syst. Struct.* **2011**, *22*(17), 2009.

[16] Ni T, Zuo L, Kareem A. Assessment of energy potential and vibration mitigation of regenerative tuned mass dampers on wind excited tall buildings. *Proceedings of ASME 2011 International Design Engineering Technical Conferences & Computers and Information in Engineering Conference*, IDETC/CIE 2011, Washington DC, USA **2011**.

[17] W. A. Shen, S. Zhu, Y. L. Xu, *Sens. Actuators, A* **2012**, *180*, 166.

[18] R. L. Harne, *App. Math. Model.* **2013**, *37*(6), 4360.

[19] A. Gonzalez-Buelga, L. R. Clare, A. Cammarano, S. A. Neild, S. G. Burrow, D. J. Inman, *Struct. Control Health Monit.* **2014**, *21*(8), 1154.

[20] L. Zuo, C. Wen, *J. Vib. Acoust.* **2013**, *135*(5), 051018-1-9.

[21] X. Tang, L. Zuo, *J. Intell. Mater. Syst. Struct.* **2012**, *23*(18), 2117.

[22] P. Bisegna, G. Caruso, G. Vairo, *J. Intell. Mater. Syst. Struct.* **2013**, *25*(13), 1553.

[23] A. Gonzalez-Buelga, L. Clare, S. Neild, S. Burrow, D. Inman, *Struct. Control Health Monit.* **2015**, *22*(11), 1359.

[24] K. Takeya, E. Sasaki, Y. Kobayashi, *J. Sound Vib.* **2016**, *361*, 50.

[25] Palomera-Arias R. Passive electromagnetic damping device for motion control of building structures, Ph.D. Dissertation, Massachusetts Institute of Technology, USA **2005**.

[26] R. Palomera-Arias, J. J. Connor, J. A. Ochsendorf, *J. Struct. Eng. ASCE* **2008**, *134*(1), 164.

[27] S. Zhu, W. A. Shen, Y. L. Xu, *Eng. Struct.* **2012**, *34*, 198.

[28] Shen W. Electromagnetic damping and energy harvesting devices in civil structures, Ph.D. Dissertation, The Hong Kong Polytechnic University, Hong Kong **2014**.

[29] Arsem HB. Electric shock absorber, United States Patent Office, USA **1971**.

[30] M. R. Jolly, D. L. Margolis, *J. Vib. Acoust.* **1997**, *119*(2), 208.

[31] Graves KE. Electromagnetic energy regenerative vibration damping. Ph.D. Dissertation, Swinburne University of Technology, Australia **2000**.

[32] B. Ebrahimi, H. Bolandhemmat, M. B. Khamesee, F. Golnaraghi, *Veh. Syst. Dyn.* **2011**, *49*(1–2), 311.

[33] S. S. Kim, Y. Okada, *J. Vib. Acoust.* **2002**, *124*(1), 110.

[34] B. L. Gysen, J. J. Paulides, J. L. Janssen, E. A. Lomonova, *IEEE Trans. Veh. Technol.* **2010**, *59*(3), 1156.

[35] C. B. Williams, R. B. Yates, *Sens. Actuators, A* **1996**, *52*(1–3), 8.

[36] P. D. Mitcheson, T. C. Green, E. M. Yeatman, A. S. Holmes, *J. Microelectromech. Syst.* **2004**, *13*(3), 429.

[37] S. P. Beeby, M. J. Tudor, N. M. White, *Meas. Sci. Technol.* **2006**, *17*(12), 175.

[38] N. G. Stephen, *J. Sound Vib.* **2006**, *293*(1–2), 409.

[39] F. Casciati, R. Rossi, *Struct. Control Health Monit.* **2007**, *14*(4), 649.

[40] W. Shen, S. Zhu, H. Zhu, Y. L. Xu, *Smart Struct. Syst.* **2016**, *18*(3), 449.

[41] W. Shen, S. Zhu, *J. Intell. Mater. Syst. Struct.* **2015**, *26*(1), 3.

[42] R. W. Erickson, D. Maksimovic, *Fundamentals of power electronics*, Springer, Berlin, Germany **2001**.

[43] G. D. Szarka, B. H. Stark, S. G. Burrow, *IEEE Trans. Power Electron.* **2012**, *27*(2), 803.

[44] E. Lefeuvre, D. Audigier, C. Richard, D. Guyomar, *IEEE Trans. Power Electron.* **2007**, *22*(5), 2018.

[45] R. D′hulst, T. Sterken, R. Puers, G. Deconinck, J. Driesen, *IEEE Trans. Ind. Electron.* **2010**, *57*(12), 4170.

[46] N. Kong, D. S. Ha, A. Erturk, D. J. Inman, *J. Intell. Mater. Syst. Struct.* **2010**, *21*(13), 1293.

[47] G. K. Ottman, H. F. Hofmann, A. C. Bhatt, G. A. Lesieutre, *IEEE Trans. Power Electron.* **2002**, *17*(5), 669.

[48] T. T. Toh, P. D. Mitcheson, A. S. Holmes, E. M. Yeatman, *J. Micromech. Microeng.* **2008**, *18*(10), 104008.

[49] J. N. Yang, A. K. Agrawal, B. Samali, J. C. Wu, *J. Eng. Mech.* **2004**, *130*(4), 437.

[50] B. Samali, K. C. S. Kwok, G. S. Wood, J. N. Yang, *J. Eng. Mech.* **2004**, *130*(4), 447.

How to cite this article: Shen W, Zhu S, Xu Y-L, Zhu H-p. Energy regenerative tuned mass dampers in high-rise buildings. *Struct Control Health Monit*. 2018;25:e2072. https://doi.org/10.1002/stc.2072